EMPIRICAL SIZE-DEPENDENT GROWTH RATE MODELS

Jerzy MYDLARZ*

Institute of Chemical Engineering and Heating Equipment,
Technical University of Wroclaw, ul. Norwida 4/6, 50—373 Wroclaw, Poland

Received October 30, 1990
Accepted May 21, 1991

A comparison of well known size-dependent crystal growth rate models has been presented. The models have been verified for crystal size distributions which have been recently presented in the literature. It is shown that for large crystal size range both the Abegg–Stevenson–Larson (ASL) model and the Canning–Randolph (C–R) model can be reduced to the simplest Bransom model. Two another kinetics size-dependent growth rate models have been presented and tested for size distributions which were recently presented by Mydlarz and Jones. Application of the proposed size-dependent growth models gives much better estimation of growth rate than other size-dependent models tested as well as Sikdar and White–Bendig–Larson methods.

The simulation, design and control of bulk suspension crystallizers is dependent on the accurate prediction of the crystal size distribution (CSD). Crystallization kinetics are commonly measured using the continuous mixed-suspension, mixed-product-removal (MSMPR) crystallizer technique which permits simultaneous determination of both growth and nucleation rates by analysis of the CSD at a given mean residence time. These kinetic data can be then correlated with appropriate growth and nucleation rate models.

For an MSMPR crystallizer operating at steady state, the general population balance equation reduces to[1]:

$$\frac{\mathrm{d}[G(L) \,.\, n(L)]}{\mathrm{d}L} + \frac{n(L)}{\tau} = 0 \qquad (1)$$

where $G(L)$ is the crystal growth rate, $n(L)$ is the population density, L is the crystal size and τ is the mean retention time of suspension within the crystallizer. For size-independent growth $G(L) = G$ = constant, Eq. (1) can be integrated to give:

$$n(L) = n^0 \,.\, \exp\left[-L/(G \,.\, \tau)\right] \qquad (2)$$

* Present address: Department of Chemical Engineering, Michigan State University, East Lansing, MI 48824—1226, U.S.A.

Eq. (2) indicates that a size analysis performed on a representative sample of crystallizer contents yields the necessary data to determine both crystal growth rate G $(= dL/dt)$, and nuclei population density n^0 $(L = 0)$, the latter being related to the nucleation rate B^0 $(= n^0 . G)$.

Non-constant growth rates complicate the determination of kinetics from CSD data. Researches have used several approaches to dealing with the modelling of non-constant growth. These include size-dependent growth and growth rate dispersion; experimental data show the existence of both size-dependent growth and growth rate dispersion. Mydlarz[2] and Mydlarz and Briedis[3,4] has recently compared the size-dependent and growth rate dispersion modelling of growth rate estimation for MSMPR crystallizer CSD data, using both current known empirical size-dependent and growth dispersion models. They found[2-4] that the size-dependent growth rate modelling remains , at present, the recommended approach for modelling growth rate kinetics for MSMPR crystallizer CSD data.

When crystal growth rate is size-dependent, relationships between crystal size distribution and crystallization kinetics become more complicated. Three general methods have been proposed in the literature for estimation of size-dependent growth rate from continuous mixed-suspension, mixed product-removal (MSMPR) crystallizer.

Briefly, discrete values of the size-dependent growth rate can be estimated from equation suggested by Sikdar[5] (Method I):

$$G(L) = \frac{N(L)}{\tau . (nL)} \tag{3}$$

where $N(L)$ is the cumulative number oversize distribution defined by:

$$N(L) = \int_L^\infty n(L)\, dL; \quad \frac{dN(L)}{dL} = -n(L) \tag{4}$$

The second method of growth rate estimation for MSMPR crystallizer CSD data is facilitated by application of well known equation (Method II: White–Bendig–Larson[6]; WBL)

$$\frac{d \ln N(L)}{dL} = \frac{-1}{\tau . G(L)} \tag{5}$$

Eq. (5) thus permits determination of growth rate from the slope of $\ln N(L)$. Note that Eq. (5) is true whether the growth rate varies with size or not.

The third methods (Method III) employs empirical size-dependent growth models used in conjunction with population balance (Eq. (1)). The equations derived represents the variation of population density or cumulative number oversize with size for an MSMPR crystallizer explicitly.

EMPIRICAL SIZE-DEPENDENT GROWTH MODELS

Several empirical size-dependent growth models are available in the literature; linear, power, hyperbolic and exponential models are most frequently used.

Power Models

The most notable are those proposed by:

1) Bransom[7]

$$G_B(L) = a_B \,.\, L^{b_B} \tag{6}$$

2) Canning and Randolph[8] (C–R)

$$G_C(L) = G_C^0 \,.\, (1 + a_C L^{b_C}) \tag{7}$$

3) Abegg, Stevens and Larson[9] (ASL)

$$G_A(L) = G_A^0 \,.\, (1 + a_A L)^{b_A} \tag{8}$$

where G^0 is the growth rate at zero size while a, b, and c are the empirical parameters. All the models presented above predict infinite growth rates as $L \Rightarrow \infty$ which is, of course, physically unrealizable. Additionally, Bransom's model predicts zero values of G as $L \Rightarrow 0$.

Exponential Models

Rosen and Hulburt, for the first time, proposed exponential dependence of crystal size on crystal growth rate growing in fluidized bed crystallizer, which in the case of constant supersaturation, can be written as[10]:

$$G(L) = k_1 \,.\, (1 - k_2 \,.\, e^{-k_3 v}) \tag{9}$$

where k_1, k_2, k_3 are parameters and v is the velocity of fluidizing supersaturated solution. It is clear that fluid velocity, v, is a function of crystal size, L.

Rojkowski proposed another exponential model[11]:

$$G(L) = G_1 - (G_1 - G^0) \,.\, \exp(-a_R \,.\, L) \tag{10}$$

where G_1 is the limiting growth rate for large crystals, G^0 is the growth rate of crystal at zero size while a is the empirical parameter. Note that Eq. (*10*) can be written in the form:

$$G(L) = G_1 \left(1 - \frac{G_1 - G^0}{G_1} \,.\, \exp(-a_R L)\right) \tag{11}$$

which refers exactly to the Rosen and Hulburt model (Eq. (9)): $k_1 = G_1$, $k_2 = (G_1 - G^0)/G_1$, and $k_3 = a_R$.

Using the Rojkowski model (Eq. (10)) with the population balance concept (Eq. (1)) a steady-state population density distribution is obtained[11]:

$$n(L) = \frac{N^0}{\tau \,.\, G^0} \left(\frac{G_1 - \Delta G}{G_1 - \Delta G \,.\, \exp(-a_R L)} \right)^{1 + (1/\tau a_R G_1)} \exp\left[-L/(\tau G_1) \right] ; \quad \Delta G = G_1 - G^0 \tag{12}$$

Hyperbolic Models

There are two hyperbolic size-dependent growth rate models available in the literature:

1) Baumann's model[12]:

$$G(L) = G_1 \,.\, \frac{L - a_2}{L + a_3} \tag{13}$$

where $G(L)$ is equal to zero for $a_2 = 0$. For crystals of large size, however, $G(L)$ asymptotically approaches limiting growth rate, G_1.

2) Rojkowski's model[11]:

$$G(L) = \frac{G^0 + \beta G_1 L}{1 + \beta L} \tag{14}$$

where G_1 and G^0 have the same meanings as in Eq. (10), while β is the parameter of the model.

Both the Baumann model (Eq. (13)) and Rojkowski (Eqs (10) and (14)) models satisfy all essential requirements for size-dependent growth model, i.e. yield finite values of $G(L)$ for very large crystal sizes, and positive and non-zero values of growth rate for crystal of zero size. Note that Rojkowski hyperbolic model (Eq. (14)) can be written in the form:

$$G(L) = G_1 \left(\frac{L + G^0/(\beta G_1)}{L + 1/\beta} \right) \tag{15}$$

which exactly refers to the Baumann model (Eq. (13)): $-a_2 = G^0/(\beta G_1)$, $a_3 = 1/\beta$.

Two other growth models: two (MJ-2) and three (MJ-3) parameter exponential size-dependent growth models have been recently proposed by Mydlarz and Jones[13,14,15] (see later).

The mentioned above size-dependent models will be examined for the potash alum MSMPR crystallizer CSD data[16] which are again presented in Fig. 1. The experimental conditions are presented in this figure. The discrete values of crystal growth rates were estimated by using WBL method.

If the data points are used directly, the growth rate calculated using the WBL method (Eq. 5) is given by:

$$G(L_i, L_{i-1}) = G(\bar{L}_i) = \frac{L_{i-1} - L_i}{\tau \cdot \ln\left(\frac{N(L_i)}{N(L_{i-1})}\right)} \qquad (16)$$

where $\bar{L}_i$ is the arithmetic average crystal size in the range L_i, L_{i-1}, and the subscripts i and $i-1$ refer to the two consecutive sizes ($L_i < L_{i-1}$), $N(L_i)$ is the cumulative number oversize distribution.

The population density data shown in Fig. 1 were recalculated as cumulative number oversize distribution data using following expression:

$$N(L_i) = \sum_{i=2}^{n} [n(\bar{L}_i) \cdot (L_{i-1} - L_i)] \qquad (17)$$

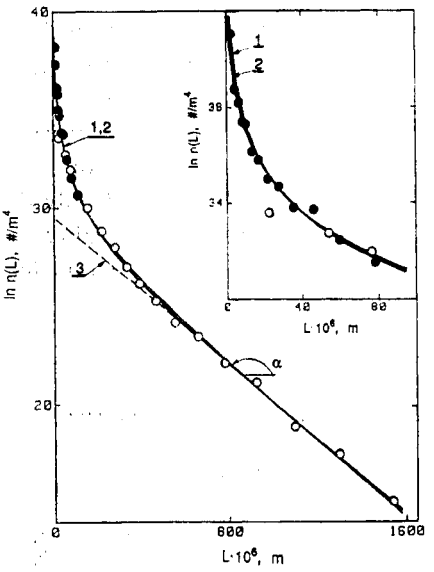

FIG. 1

CSD of potash alum crystallized by continuous cooling crystallization in MSMPR crystallizer (Jones and Mydlarz, 1990). 1 MJ-2 (Eq. (*25*)); 2 MJ-3 (Eq. (*31*)); 3 linear regression for crystals larger than about 350 μm, $\mathrm{tg}(\alpha)$ = slope = $-9{\cdot}471 \cdot 10^3$ m^{-1}

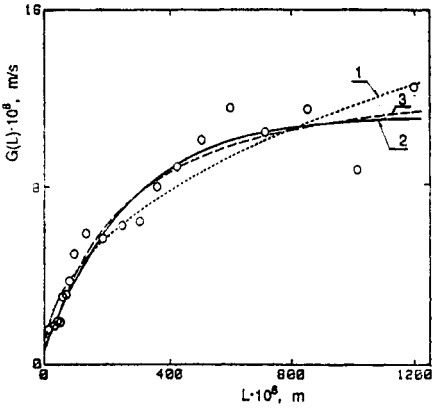

FIG. 2

Correlation of potash alum growth rate calculated by the White–Bending–Larson method by means of the Bransom, C–R, ASL and Rojkowski models. 1 Eqs (*6*, *7*, *8*); 2 Eq. (*10*); 3 Eq. (*14*)

where $n(\bar{L}_i)$ is the value of $n(L)$ at the midpoint $\bar{L}_i$ of a size range $L_{i-1} - L_i$. The discrete potash alum crystal growth rates estimated from Eq. (*16*) were then fitted to the empirical size-dependent models (Eqs (*6*), (*7*), (*8*), (*10*) and (*14*)). Parameter values obtained are presented in Table I. Graphical interpretation of these correlation is presented in Fig. 2. Values of the mean square error, S_y, are also presented in Table I. S_y was calculated from the equation:

$$S_y = 100 \cdot \left[\frac{\sum_{i=1}^{k} \left[\frac{G_i - G_c}{G_i} \right]^2}{k} \right]^{1/2} \qquad (18)$$

where G_i is the estimated (using WBL method) value of $G(L)$, G_c is the value of these quantity calculated from size-dependent growth model, and k is the number of experimental data points.

Analysis of the results presented in Table I and Fig. 2 lead to conclusion that graphical illustration of Branson, C–R and ASL models are practically the same. It was noted that values of parameters "a" and "G^0" in Eqs (7) and (8) are related to their initial guesses, while the value of parameter "b" remains essentially constant. Due this fact, the discrete values of $G(L)$ evaluated using WBL method were again fitted to the C–R and ASL models assuming constant values of parameter "a". Results of this exercise are presented in Table II. It is clear from Table II that value of G^0 is related to the assumed value of parameter "a". Note that values of mean square error, S_y, variance of fit, δ, and weighted sum of squares are practically the same for the each set of parameters (G^0, a, b). It means that quality of correlation considered size-dependent models for each set of parameters

TABLE I

Comparison of the empirical size-dependent crystal growth models for potash alum data

Model	Model parameters					
	a μm^{-1}	b —	$G^0 \cdot 10^9$ $m\,s^{-1}$	$G_1 \cdot 10^8$ $m\,s^{-1}$	$\beta \cdot 10^3$ μm^{-1}	S_y %
$G(L) = a \cdot L^b$	$0{\cdot}55 \cdot 10^{-8}$	0·442	0	—	—	22·10
$G(L) = G^0(1 + aL^b)$	1·407	0·427	4·182	—	—	26·51
$G(L) = G^0(1 + aL)^b$	1·069	0·434	5·662	—	—	22·60
$G(L) = G_1 - (G_1 - G^0)\,e^{-aL}$	0·00373	—	7·446	11·200	—	14·37
$G(L) = \dfrac{G^0 + \beta G_1 L}{1 + \beta L}$	—	—	2·110	13·562	4·339	12·10

$((G_C^0, a_C, b_C); (G_A^0, a_A, b_A))$ is very similar. It is easy to show that in each case:

$$1 + a_C L^{b_C} \simeq a_C L^{b_C} \tag{19}$$

$$1 + a_A L^{b_A} \simeq a_A L^{b_A} \tag{20}$$

because $a_C L^{b_C} \gg 1$ and $a_A L^{b_A} \gg 1$. Thus, we can further confirm the following equation:

$$G_B(L) \cong G_C(L) \cong G_A(L) = a_B L^{b_B} \tag{21}$$

The same conclusion can be drawn analyzing the values of parameters presented in Table II. For each set of model parameters (a_C, G_C^0, b_C or a_A, G_A^0, b_A) the following relationship is valid:

$$a_C G_C^0 \cong a_A G_A^0 \cong a_B \tag{22}$$

These results confirms that despite the fact that the C–R and ASL are predict growth rate for crystals of zero size, these values should be treated with caution, however, when extrapolated from CSD data for larger crystals size range.

DIRECT ESTIMATION OF GROWTH RATE FOR MSMPR CRYSTALLIZER CSD DATA (METHOD III)

As mentioned earlier in this paper, an alternative – direct method – permits estimation of size-dependent growth rate. This procedure (Method III) employs empirical

TABLE II

Parameters of size-dependent crystal growth rate models for potash alum

a	Canning–Radolph model (C–R) Eq. (7)					Abegg–Steves–Larson model (ASL) Eq. (8)				
μm^{-1}	G_C^0 m/s	b_C –	S_y %	δ^2 m^2/s	S_b m^2/s	G_A m/s	b_A –	S_y %	δ^2 m^2/s	S_b m^2/s
0·1	$1{\cdot}545 \cdot 10^{-8}$	0·609	26·62	35·13	1·76	$1{\cdot}362 \cdot 10^{-8}$	0·467	24·08	28·31	1·42
0·5	$6{\cdot}855 \cdot 10^{-9}$	0·504	23·84	28·63	1·43	$7{\cdot}265 \cdot 10^{-9}$	0·448	22·56	26·03	1·30
1·0	$4{\cdot}185 \cdot 10^{-9}$	0·478	23·12	27·22	1·36	$5{\cdot}434 \cdot 10^{-9}$	0·445	22·35	25·73	1·29
10·0	$5{\cdot}357 \cdot 10^{-10}$	0·446	22·24	25·63	1·28	$1{\cdot}995 \cdot 10^{-9}$	0·442	22·12	25·46	1·27
50·0	$1{\cdot}099 \cdot 10^{-10}$	0·443	22·14	25·47	1·27	$9{\cdot}817 \cdot 10^{-10}$	0·442	22·11	25·43	1·27
10^2	$5{\cdot}518 \cdot 10^{-11}$	0·442	22·12	25·44	1·27	$7{\cdot}229 \cdot 10^{-10}$	0·442	22·11	25·43	1·27
10^3	$5{\cdot}535 \cdot 10^{-12}$	0·442	22·11	25·43	1·27	$2{\cdot}605 \cdot 10^{-10}$	0·442	22·09	25·42	1·27
10^6	$5{\cdot}537 \cdot 10^{-14}$	0·442	22·11	25·42	1·27	$3{\cdot}399 \cdot 10^{-11}$	0·442	22·09	25·42	1·27
10^{10}	$5{\cdot}537 \cdot 10^{-19}$	0·442	22·11	25·42	1·27	$2{\cdot}090 \cdot 10^{-13}$	0·442	22·11	25·42	1·27

size-dependent growth models used in conjunction with the population balance (Eq. (*1*)). The equation derived represent the variation of population density or cumulative number oversize distributions for an MSMPR crystallizer explicitly. Direct fitting of the experimental CSD data to this derived equations permits estimation of size-dependent crystal growth rate.

The requirements of size-dependent growth model should conform to the following:

1. It should fit the experimental data well in as wide a range of sizes as possible,
2. It should be physically realizable, that is, it should yield finite, positive and non-zero values for growth rate for very small and very large crystal sizes,
3. It should have a number of parameters which can be determined easily from experiments,
4. It should be of a reasonable simple form, so that it can treated theoretically with ease.

Two Parameter Exponential Model (MJ-2)

Recently, Mydlarz and Jones[13,14] proposed a simple exponential two-parameter size-dependent growth model (MJ-2):

$$G(L) = G_m(1 - e^{-aL}) \tag{23}$$

where G_m is the limiting growth rate for large crystals, L is the crystal size and "a" is an empirical parameter. Application of the MJ-2 model for potash alum crystals produced in an MSMPR crystallizer showed that G_m is an increasing function of supersaturation while while value of parameter "a" remains essentially constant for a given system[2]. Growth rate $G(L)$ approaches limiting values of G_m for $L \Rightarrow L_{max}$ and zero for $L = 0$. This latter condition can present conceptual difficulties, however, in deducting the nucleation rates, B^0.

Zero-size growth is a mathematical concept which is frequently used in estimation nucleation rates. Thus the zero-size nucleation rate, B^0, is usually expressed in terms of nuclei density, n^0, and zero-size growth rate, G^0 and difficulty clearly arises if G^0 equals zero. Nevertheless, Jančič and Garside[17] showed that the nucleation rate can also be calculated from the mean residence time, τ, and population density data only:

$$B^0 = \frac{N_T}{\tau} = \frac{1}{\tau} \cdot \int_0^\infty n(L)\, dL = n^0 G^0 \tag{24}$$

Thus the zero-size growth rate can be estimated using Eq. (*20*), which is valid for both size-dependent and size-independent growth processes. Despite the fact that the MJ-2 model does not predict zero-size growth rate, it does give a satisfactory fit

of author's experimental data[14,18] and of available in the literature MSMPR crystallizer CSD data[2].

Using the MJ-2 model (Eq. (*23*)) with the population balance concept (Eq. (*1*)) a simple steady-state population density and cumulative number oversize distributions is obtained[13,14]:

$$\ln n(L) = \ln (n^*) + . a(L - L^*) + \frac{-1 - b}{b}\left(\frac{e^{aL} - 1}{e^{aL^*} - 1}\right) : b > 0 ; \quad b = aG_m\tau \qquad (25)$$

or

$$\ln N(L) = \ln (N^*) + \frac{-1}{b}\left(\frac{e^{aL} - 1}{e^{aL^*} - 1}\right) \qquad (26)$$

where the superscript * refers to a chosen size crystal L^* and corresponding population density n^* or cumulative number oversize distribution N^*. Note that Eqs (*25*) and (*26*) contain only two parameters (a and b, respectively), thus these equations permits of the parameter of the MJ-2 model from the MSMPR crystallizer CSD data in a simple way. Although Eqs (*25*) and (*26*) do not predict the population density and cumulative number oversize distributions at zero size, it is possible to choose value of L^* arbitrarily close to zero. In the practical application of Eqs (*25, 26*), L^* is the smallest measured crystal size which is dependent on the measured technique used.

Substitution of MJ-2 model (Eq. (*23*)) into population balance (Eq. (*1*)) and than integration in limits from unknown L_N to L yields:

$$\ln n(L) = \ln (n_N) + . a(L - L_N) + \frac{-1 - b}{b}\left(\frac{e^{aL} - 1}{e^{aL_N} - 1}\right) \qquad (27)$$

or

$$\ln N(L) = \ln (N_N) + \frac{-1}{b}\left(\frac{e^{aL} - 1}{e^{aL_N} - 1}\right) \qquad (28)$$

where L_N is the size of the smallest nuclei produced in the MSMPR crystallizer and $n_N(N_N)$ is the population density (cumulation number oversize) of nuclei. Note that Eq. (*27*) and Eq. (*28*) contain four adjustable parameters: a, b, L_N, $\ln (n_N)$ (Eq. (*27*)); a, b, L_N, $\ln (N_N)$ (Eq. (*28*)). Thus, fitting experimental MSMPR crystallizer CSD data to Eqs (*27*) or (*28*) permits not only estimation of parameter of the MJ-2 model (a and b, respectively), but also permits evaluation of nuclei size, L_N, and its population density, n_N (or cumulative number oversize distribution, N_N), and further the nucleation kinetics:

$$B_N = n_N . G_N \qquad (29)$$

where $G_N = G(L = L_N) = G_m(1 - e^{-a.L_N})$.

Three Parameter Exponential Model (MJ-3)

Mydlarz and Jones suggested recently three parameter exponential size-dependent growth model (MJ-3)[15,19]:

$$G(L) = G_m(1 - e^{-a(L+c)}) \tag{30}$$

where G_m and a have the same meaning as in Eq. (*24*), while "c" is additional empirical parameter. It can be shown[2,20] that the MJ-3 model is a simpler form of the Rojkowski exponential model (Eq. (*10*)). Using the MJ-3 model with population balance concept (Eq. (*1*)), a simple steady-state population density, $n(L)$, and cumulative number oversize, $N(L)$, distributions are simply obtained[15,19]:

$$n(L) = K \,.\, e^{aL} \,.\, (A \,.\, e^{aL} - 1)^{(-1-b)/b} :$$

$$b = aG_m\tau \,; \quad A = e^{ac} \,; \quad K = n^0(A - 1)^{(1+b)/b} \tag{31}$$

$$N(L) = K_N \,.\, (A \,.\, e^{aL} - 1)^{-1/b} \quad : K_N = N^0(A - 1)^{(1+b)/b} \tag{32}$$

For potassium sulfate and potash alum data[2], parameter "c" is equal to about 1 μm, while parameter "a" is about 10^4 m^{-1}, thus parameter A is close to unity ($A \cong 1{\cdot}02$).

The MJ-2 and MJ-3 model have been presented in details elsewhere[13–15,19].

Application of the MJ-2 and MJ-3 Size-Dependent Models

The MJ-2 and MJ-3 growth rate models will be examined for use in the estimation of $G(L)$ for two set of simulated data of known characteristic as used previously[16] and in correlation of real available in the literature.

Simulated Data

The first set of simulated data is derived from the linear relation:

$$\ln n(\bar{L}) = -p\bar{L} + \ln (n^0) \tag{33}$$

with $p = 1{\cdot}25 \,.\, 10^4$ m^{-1} and $\ln (n^0) = 34$.

The second set exhibits a significant curvature and is calculated from the following equation:

$$\ln n(\bar{L}) = P_1 \,.\, \exp (P_2 \,.\, L^{-0{\cdot}5} + P_3 \,.\, \bar{L}) + P_4 \,.\, \bar{L} + P_5 \tag{34}$$

with $P_1 = 29{\cdot}3071$, $P_2 = -134{\cdot}882$ m$^{-1/2}$, $P_3 = 1\,820{\cdot}21$ m^{-1}, $P_4 = -1{\cdot}25 \,.\, 10^4$ m^{-1} and $P_5 = 24{\cdot}4516$. A residence of time of 1 000 s will be assumed in each case. The simulated population density data described by Eqs (*33*) and (*34*) are also presented in Fig. 3. Note (Table I in ref.[16]) that $\bar{L}$ in Eqs (*33*) and (*34*) refers to typical values from a standard sieve test.

Direct fitting of the first set of population density CSD data (Eq. (*33*)) to the Eqs (*25*, *31*) results in the value of parameters which are presented in Table III. Note that in the case when log population density data plot is a linear function of size the values of parameter "*a*" is approximately two order of magnitude larger than in the case when log population data plot exhibits a significant curvature (Eq. (*34*)) (see Table III). It is easy to show that for such larger values of parameter "*a*" Eq. (*25*) and Eq. (*31*) reduce to a respectively simpler form:

$$n(L) = n^* \cdot \exp\left(\frac{-a}{b}(L - L^*)\right) \tag{35}$$

$$n(L) = n^0 \cdot \exp\left(\frac{-a}{b} \cdot L\right) \tag{36}$$

e.i. to the expected form for MSMPR crystallizer CSD data when growth rate is size-independent (see Eq. (*2*)). In such cases the $G(L)$ can be easily estimated from the slope of the log population density vs size data plot.

Direct fitting of the second set of population density CSD data (Eq. (*30*)) to the Eqs (*25*, *31*) results in the value of parameters which are presented in Table III. Note that both the MJ-2 and MJ-3 model predict practically exactly theoretical values of $G(L)$ in the case when log population density exhibits significant curvature (Eq. (*34*)) (see Fig. 4). The theoretical values of $G(L)$ for the CSD data represented

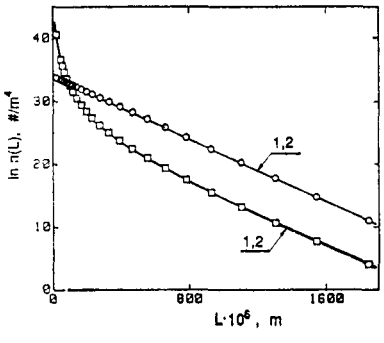

FIG. 3

Graphical interpretation of Eqs (*33*, *34*). ○ Eq. (*33*); □ Eq. (*34*); 1 MJ-2 (Eq. (*25*)); 2 MJ-3 (Eq. (*31*))

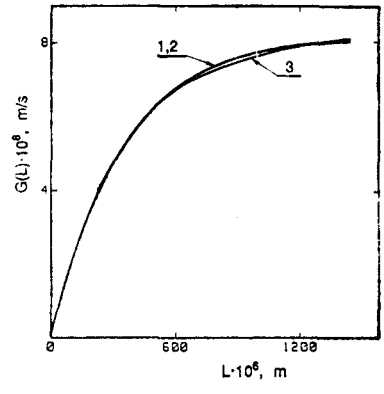

FIG. 4

Comparison of theoretical size-dependent growth rate with that predicted by the MJ-2 and MJ-3 model. 1 MJ-2 ((Eq. *23*)); 2 MJ-3 (Eq. (*30*)); 3 Eq. (*3*)

TABLE III

Constant of the MJ-2 and MJ-3 size-dependend growth models

Model	Parameters										
	$L^* \cdot 10^6$ m	$\ln(n^*)$ m^{-4}	$L_N \cdot 10^6$ m	$\ln(n_N)$ m^{-4}	$\ln(n^0)$ m^{-4}	$a \cdot 10^{-3}$ m^{-1}	b —	$c \cdot 10^6$ m	$G^0 \cdot 10^{10}$ m	$G_N \cdot 10^9$ m/s	$G_m \cdot 10^8$ m/s
$\ln n(L) = -1{\cdot}25 \cdot 10^4 \cdot L + 34$											
$G(L) = G_m(1 - e^{-aL})$	22	33·725	—	—	—	385·47	30·840	—	0	—	8·000
$G(L) = G_m[1 - e^{-a(L+c)}]$	—	—	—	—	34·00	28·286	2·263	2·263	799·99	—	8·000
$\ln n(L) = 29{\cdot}3071 \cdot \exp(-134{\cdot}882 \cdot L^{1/2} + 1\,820{\cdot}21 \cdot L - 1{\cdot}25 \cdot 10^4 \cdot L + 24{\cdot}4516$											
$G(L) = G_m(1 - e^{-aL})$	22	40·380	—	—		2·994	0·244	—	0	—	8·140
	—	—	0·997	56·462	—	2·981	0·242	—	0	2·407	8·114
$G(L) = G_m[1 - e^{-a(L+c)}]$	—	—	—	—	57·067	2·927	0·239	0·945	0·225	—	8·154
Run 18: $KAl(SO)_4.12\,H_2O$											
$G(L) = G_m(1 - e^{-aL})$	10·5	37·309	—	—	—	5·438	0·578	—	0	—	10·187
	—	—	1·073	43·033	—	5·866	0·615	—	0	6·301	10·187
$G(L) = G_m[1 - e^{-a(L+c)}]$	—	—	—	—	42·502	5·447	0·572	1·696	0·926	—	10·066
Run: $AlNH_4(SO_4).12\,H_2O$											
$G(L) = G_m(1 - e^{-aL})$	5·84	37·771	—	—	—	9·678	1·009	—	0	—	9·14
	—	—	0·895	41·491	—	9·713	1·012	—	—	0·79	9·14
$G(L) = G_m[1 - e^{-a(L+c)}]$	—	—	—	—	38·976	7·039	0·787	5·466	37·00	—	9·81

by Eq. (*34*) were calculated from the Sikdar equation (Eq. (*3*)) which may be written in the form:

$$G(L) = \frac{\int_0^L n(L)\,\mathrm{d}L}{\tau \,.\, n(L)} \qquad (37)$$

The integrals in Eq. (*37*) were evaluated numerically using Simpson's rule (step = = 1 μm). It is also interesting to note that, in both cases of simulated CSD data, use of Eqs (*25*, *31*) with parameter values listed in Table III, reproduces the population density data represented by Eqs (*33*) and (*34*), respectively with excellent agreement as illustrated in Fig. 3.

Experimental Data

The MJ-2 and MJ-3 growth rate models will be further examined for use in the estimation of $G(L)$ for experimental data of potash alum[16] (Fig. 1). The experimental potash alum data (Fig. 1) were fitted to MJ-2 (Eq. (*25*)) and MJ-3 (Eq. (*31*)) theoretical population distribution curves. The results of these fitting are presented in Table III. It is interesting to note that log population density data for crystals larger than about 350 μm are approximately linear (see Fig. 1). Thus in this size range the growth rate is practically size-independent and can be easily estimated from the slope of the log population density data plot ($-1/\tau G_{max}$) and the mean residence time τ. Linear regression of the log population density data for crystal larger than about 350 μm results in a slope equal to $-9{\cdot}471 \,.\, 10^3\ \mathrm{m}^{-1}$. With $\tau = 1\,044$ s, the maximum growth rate, G_{max}, should approach a value of $0{\cdot}101\ \mu\mathrm{m\ s}^{-1}$.

The directly estimated size-dependent growth kinetic of potash alum are also presented in Fig. 5. The predictions of the MJ-2 and MJ-3 models are quite similar and show a size-dependent behavior in which the growth rate continues to increase with increasing size asymptotically to a maximum. It should emphasized here that the predictions of the MJ-2 and MJ-3 models in the larger crystal size range are consistent with the maximum growth rate, G_{max}, obtained from the slope of log population density data plot. Use of the C–R, ASL and Rojkowski models for discrete $G(L)$ calculated using WBL equation (Method II), however, shows increasing deviation in growth rate with increasing crystal size (see Fig. 5).

The experimental potash alum data reported recently by Jones and Mydlarz[18] were also fitted to MJ-2 (Eq. (*27*)) theoretical population distribution curve. Fig. 6 shows the estimated nuclei size, L_N, as a function of relative supersaturation, σ. As can be seen from this figure, the estimated nuclei size, L_N, is significantly related to the actual level of supersaturation. The higher the supersaturation, the smaller is the nuclei size. This relation is consistent with theoretical prediction[21].

Fig. 7 shows aluminum–ammonium alum continuous population density data reported by Rojkowski[11]. The experimental conditions are presented in this figure. Again it should be noted that the log population data presented in Fig. 7 for crystal larger than 231 μm are approximately linear with size. Estimated from the slope of log population density data the maximum growth rate, G_{max}, is equal to 0·098 μm s^{-1}.

The fits of the Rojkowski population density curve (Eq. (*12*)) to the sieving log population density data are presented in Fig. 7. The curve is based on the best values of a, n^0, G_1 and G^0 reorted by Rojkowski ($a = 3{\cdot}2 \cdot 10^{-3}$ μm^{-1}, $G^0 = 0{\cdot}018$ μm . . s^{-1}, $G_1 = 0{\cdot}117$ μm s^{-1}, $B^0 = 10^5$ s^{-1} l^{-1}, $n^0 = B^0/G^0 = 5{\cdot}6 \cdot 10^6$ μm^{-1} l^{-1}). The theoretical Rojkowski curve obtained by using non-linear regression[11] does not fit the experimental points in the small crystal size range as well as is shown in Fig.7. This is due to the inability of the model (*10*) to fit data which exhibits significant curvature when plotted as log population vs size[11].

The data presented in Fig. 7 were also fitted to the MJ-2 and MJ-3 steady-state population density distributions (Eqs (*25*) and (*31*), respectively). Values of the model parameter calculated using a nonlinear regression are presented in Table III. The best fit ln $n(L)$ curve are also shown in Fig. 7. These lines smooth the experimental points very well for all crystal sizes.

It is interesting to compare the growth rates obtained from data presented in Fig. 7 by direct fitting these data to MJ-2 and MJ-3 steady-state distributions (Eqs (*25*) and (*31*), respectively) with growth rates reported by Rojkowski[11]. This is presented in Fig. 8. It should be noted that predictions of the MJ-2 and MJ-3 models are consistent with the value of G_{max}, obtained from the slope of log population data for crystals larger than about 231 μm. Growth rates reported by Rojkowski, however, are significantly larger than G_{max} in this crystal size range.

Similarly, there is a significant difference in prediction of zero-size population density n^0. Value of n^0 reported by Rojkowski is about one order of magnitude smaller than n^0 predicted by the MJ-3 model. Consequently, there is also a difference in prediction of nucleation rate. Use of the MJ-3 model gives $B^0 \cong 3{\cdot}1 \cdot 10^5$ #/(s l) while the nucleation rate reported by Rojkowski is equal to about $1{\cdot}0 \cdot 10^5$ #/(s l).

CONCLUSIONS

The first part of this paper has been primarily concerned with the examination of different empirical size-dependent growth rate models for potash alum data presented in paper[16]. Comparison of different growth rate models for potash alum growth rate vs size data, calculated using WBL-method shows, that both the C–R and ASL model can be reduced for simpler Bransom model. These results confirms that despite the fact that the C–R and ASL are predict growth rate for crystals of zero size, these values should be treated with caution, however, when extrapolated from CSD data for larger crystals size range.

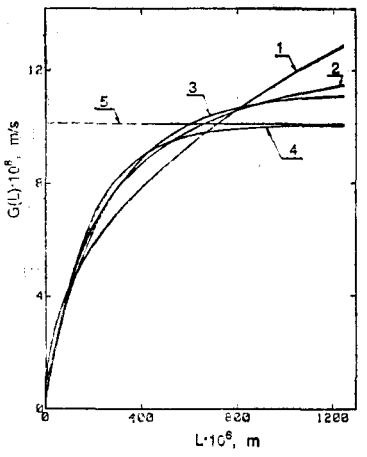

FIG. 5

Comparison of method II and method III of potash alum growth rate estimation. 1 Eqs (*6*, *7*, *8*); 2 Eq. (*14*); 3 Eq. (*10*); 4 Eqs (*23*, *30*); 5 $G_{max} = 0{\cdot}101\ \mu m\ s^{-1}$

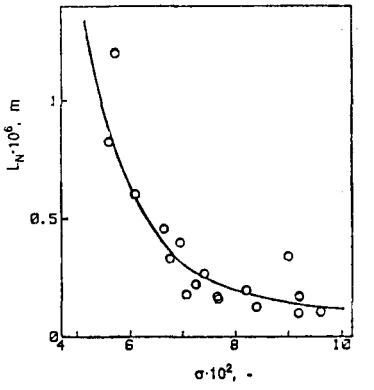

FIG. 6

Influence of supersaturation on estimated nuclei sizes

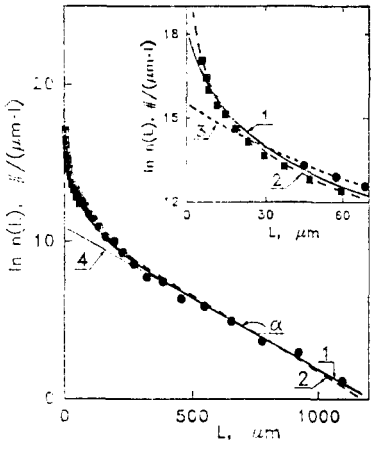

FIG. 7

Population density vs size for aluminum–ammonium alum crystals produced in an MSMPR crystallizer (Rojkowski, 1977). 1 MJ-3 (Eq. (*31*)); 2 MJ-2 (Eq. (*25*)); 3 Eq. (*12*); 4 linear regression for crystals larger than about 231 μm, $tg(\alpha)$ = slope = $-8{\cdot}99 \cdot 10^3\ m^{-1}$

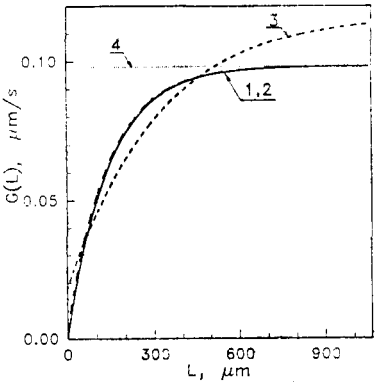

FIG. 8

Comparison of predictions of the MJ-2 and MJ-3 models with Rojkowski exponential model for aluminum–ammonium alum crystals. 1 MJ-2 (Eq. (*23*)); 2 MJ-3 (Eq. (*30*)); 3 Eq. (*10*)

In the second part of the paper the direct method of growth rate estimation for MSMPR crystallizer CSD data is discussed, and application of two other exponential size-dependent growth models (MJ-2 and MJ-3) for both simulated and experimental data is presented. The MJ-2 and MJ-3 results in both a relatively simple forms of population density distributions (Eqs (*25*) and (*31*), respectively) and cumulative number oversize distributions (Eqs (*26*) and (*32*), respectively) and also facilitates direct curve fitting of experimental log population density (or log cumulative number oversize distribution) data to determine the coefficients of the models. Additionally, the MJ-2 model allows also direct estimation of nuclei size and its population density data (Eq. (*27*)), and further the nucleation kinetics.

SYMBOLS

a, b, c	parameters of size-dependent growth models
A	parameter of the MJ-3 model
B^0	nucleation rate, $\#/(m^3\ s)$
G	linear growth rate, μm/s, m/s
G_m	limiting growth rate for large crystals, μm/s, m/s
G^0	zero-size crystal growth rate, μm/s, m/s
L	crystal size, μm, m
K, K_N	parameters of the MJ-3 model
$n(L)$	population density, $\#/m^4$
n^0	zero-size population density, $\#/m^4$
$N(L)$	cumulative number oversize distribution, $\#/m^3$
N^0	zero-size cumulative number oversize distribution, $\#/m^3$
S_b	weighted sum of squares
S_y	mean relative error, %
v	superficial velocity, m/s
Δw	supersaturation, wt % of solute
τ	mean residence time, s
δ^2	variance
σ	relative supersaturation, (—)

Subscripts

A	refers to ASL model
B	refers to Bransom model
C	refers to Canning–Randolph (C–R) model
l	refers to infinite crystal size
m	refers to large crystal size
N	refers to nuclei

Superscripts

°	refers to zero-size crystal
*	refers to crystal size $L = L^*$

REFERENCES

1. Randolph A. D., Larson M. A.: *Theory of Particulate Processes*, 2nd ed.. Academic Press, New York 1988.
2. Mydlarz J.: *Thesis.* Scientific Papers of the Institute of Chemical Engineering and Heating Equipment of Wrocław Technical University, in press.
3. Mydlarz J., Briedis D.: Comput. Chem. Eng., submitted.
4. Mydlarz J., Briedis D. in: *Industrial Crystallization* '90 (A. Mersmann, Ed.), p. 577. GVC-VDI Düsseldorf (1990a).
5. Sikdar S. K.: Ind. Eng. Chem., Fundam. *16*, 390 (1977).
6. White E. T., Bending L. L., Larson M. A.: AIChE Symp. Ser. *72*, 41 (1976).
7. Branson S. H.: Br. Chem. Eng. *5*, 838 (1960).
8. Canning T. F., Randolph A. D.: AIChE J. *13*, 5 (1967).
9. Abegg G. F., Stevens J. D., Larson M. A.: AIChE J. *14*, 188 (1968).
10. Rosen H. N., Hulburt H. M.: Chem. Eng. Prog., Symp. Ser. *67*, 27 (1971).
11. Rojkowski Z.: *Reports of the Institute of Chemical Engineering at the Warsaw Technical University.* Vol. IX, No 1 (1980).
12. Baumann K. H. in: *Industrial Crystallization '78* (E. J. de Jong and S. J. Jančić, Eds), p. 330. North-Holland, Amsterdam 1978.
13. Mydlarz J., Jones A. G.: Comput. Chem. Eng. *13*, 959 (1989).
14. Mydlarz J., Jones A. G.: Chem. Eng. Commun. *90*, 47 (1990).
15. Mydlarz J., Jones A. G.: Unpublished results.
16. Mydlarz J.: Inz. Chem. Proc., in press.
17. Jančić S. J., Garside J. in: *Industrial Crystallization '76* (J. W. Mullin, Ed.), p. 363. Plenum Press, London 1976.
18. Jones A. G., Mydlarz J.: Can. J. Chem. Eng. *68*, 250 (1990).
19. Mydlarz J., Jones A. G. in: *Industrial Crystallization '90* (A. Mersmann, Ed.), p. 417. GVC-VDI, Düsseldorf (1990c).
20. Rojkowski Z.: Private communication.
21. Mullin J. W.: *Crystallization.* Butterworths, London 1972.